The Antarctic Dipole and its Predictability

Xiaojun Yuan and Douglas G. Martinson

Lamont-Doherty Earth Observatory of Columbia University

ABSTRACT

This study investigates the nature of interannual variability of Antarctic sea ice and its relationship with the tropical climate. We find that the dominant interannual variance structure in the sea ice edge and surface air temperature fields is organized as a quasi-stationary wave which we call the "Antarctic Dipole" (ADP). It is characterized by an out-of-phase relationship between the ice and temperature anomalies in the central/eastern Pacific and Atlantic sectors of the Antarctic. The dipole consists of a strong standing mode and a weaker propagating motion within each basin's ice field. It has the same wavelength as the Antarctic Circumpolar Wave (ACW) and dominates the ACW variance. The dipole is clearly associated with tropical ENSO events; it can be predicted with moderate skill using linear regression involving surface temperature two to four months ahead. The prediction performs better in extreme warm/cold years, and best in La Niña years.

Introduction

The El Niño – Southern Oscillation (ENSO) signal has been identified in the Antarctic sea ice fields in many studies (Chu, 1983; Carleton, 1989; Simmonds and Jack, 1995; Ledley and Huang, 1997, Harangozo, 2000). A more recent study found consistent (and statistically significant) teleconnection patterns linking Antarctic sea ice edge (SIE) variations to those of tropical and mid-

latitude climate, as well as circumpolar variations amongst different polar basins (Yuan and Martinson, 2000). The strongest circumpolar teleconnection is characterized by a dipole-like pattern reflecting an out-of-phase relationship between Pacific and Atlantic polar regions, where the SIE is most responsive to extrapolar climate variability. This broad-scale covarying feature was called the Antarctic Dipole (ADP; Yuan and Martinson, 2000); it exists strongly in the surface air temperature (SAT) and SIE fields, and moderately in sea level pressure (SLP) fields. However, much of the interannual variability in the Southern Ocean has been described in the context of an Antarctic Circumpolar Wave (ACW) — a wavenumber two phenomenon propagating in ice, pressure, wind and temperature fields around the Antarctic (White and Peterson, 1996). The ACW has a period similar to the ENSO cycle. Consequently, we evaluate the variability of SIE, temperature and pressure fields in the context of standing versus propagating wave phenomena. Here we show that the ADP, a standing wave pattern (varying in time, but quasi-stationary in space), is the dominant interannual variability pattern in SIE and temperature. Moreover, we establish linear regression models to predict the ADP using its relationship with lower latitude climate variability.

Standing wave versus propagating wave

We systematically examine the Antarctic dipole as manifested in the sea ice, temperature and pressure fields. Surface air temperature and sea level pressure data from NCAR/NCEP reanalysis (Kalnay et al., 1996) were used. The SIE is derived from NASA microwave imager data (Cavalieri et al., 1997). All data were filtered to remove sub-annual variability, and means were subtracted to yield anomaly fields, indicated by a prime. The first empirical orthogonal function (EOF) mode of SIE', containing 37% of the total variance concentrated in the entire Western Hemisphere, clearly displays ths ADP phenomenon (Figure 1a). Its poles are centered within the western Amundsen Sea and central Weddell Gyre. The temporal and spatial distribution of the SIE leading mode emphasizes the dipole's nature as a standing wave (Figure 1b). In addition to SIE, it has been noted that SAT at weather stations display an out-of-phase relationship across the Antarctic Peninsula (Comiso, 2000; Harangozo, 2000). We conduct an EOF analysis on SAT' along 65°S,

which reveals the same dipole pattern. The dipole in SAT' is best defined by the combination of the first two EOF modes (figure 1c,d), containing 53% of the total variance.

To further explore the Antarctic Dipole expression in SAT and SLP, and identify its relationship with extrapolar climate, we conduct an EOF analysis on SAT' and SLP' in the Pacific and Atlantic, south of 20˚ N. The SAT' leading mode eigenvector (Figure 2a) shows a characteristic ENSO pattern with maximum amplitude centered in the central tropical Pacific. Associated with the tropical portion of this ENSO pattern is a circumpolar pattern that resembles the Antarctic Dipole in SIE', showing a pole near 60° S in the South Pacific (of like-phase to the tropical signal) and another pole of opposite phase in the Weddell Gyre. However, the SLP' leading EOF mode does not display a profound dipole, but its dominant pattern is intriguing. The leading SLP' mode shows a zonal contrast between the eastern and central tropical Pacific reflecting the Southern Oscillation, as well as a striking meridional contrast between the tropical/mid-latitude and polar/subpolar regions in the Pacific. The meridional gradient is unevenly distributed in the Pacific and more evenly distributed in the Atlantic (figure 2b). The correlation coefficient between the time series (principal components: PCs) of SAT' and SLP' leading modes is 0.67 (significant at the 99% confidence level, accounting for temporal autocorrelations existing in both PCs). The PCs capture a large portion of interannual variability between these two variables (Figure 2c).

Clearly, the Antarctic Dipole exists in both SIE and SAT anomaly fields. It is quite robust in both of the fields' total variance where it dominates the variability. Since it has the same spatial wavelength as the ACW, it is necessary to differentiate these two phenomena. The leading mode of a complex EOF (CEOF) analysis (Wallace and Dickinson, 1972; Horel, 1984) applied to the SIE' field readily describes propagating motion (Figure 3c), consistent with an ACW. It shows that the strongest portion of the ACW signal is in the eastern Pacific and Weddell Gyre sectors of the Antarctic where the ADP exists. Outside of this region weaker signals appear that propagate at different speeds in different locations. The propagating signal consists of a strong static signal (the ADP) and a weaker propagating component as well. This is apparent by examining the real EOFs

of the SIE data. The first two modes are in quadrature, with the first mode representing a standing mode or, the dipole (Figure 1a,b). The second mode contributes an eastward propagation to the dipole, and together, the primary signal of the ACW in the SIE becomes apparent. However, the propagation of the dipole signal appears to be contained within the individual basins (Figure 3a). This is also suggested by the total SIE anomaly field (Figure 3b). Moreover, when we subtract the standing mode from the total SIE' field and apply the CEOF analysis to the residual, we find the propagating signal becomes quite weak and is not consistently eastward. On the other hand, if we conduct a real EOF analysis on the CEOF leading mode (Figure 3c), the first mode is the ADP, which describes 83% of the total variance. The ADP — a standing mode with limited intra-basin eastward (on average) propagation — is the dominant mode of variability in the SIE field. A much weaker signal (approximately 20% or less of the total SIE variance) propagates outside of the dipole region and progresses around the Antarctic with the Antarctic Circumpolar Current.

Predictability of the ADP in SIE

The mechanisms responsible for the Antarctic Dipole and its link with extrapolar climate are not yet understood. We rely on the last two decades of satellite observations and reanalysis data products to statistically investigate the phenomenon. Figure 2 suggests that the Antarctic Dipole pattern is associated with interannual variability in the central tropical Pacific. We exploit this relationship to develop a linear prediction model whereby the leading mode (Figure 2c) PC of SAT (hereafter SAT-PC1), I used to forecast SIE variations associated with the ADP.

The western Amundsen Sea SIE responds strongly to extrapolar climate variability while dominating the Pacific portion of the Antarctic Dipole oscillation (Figure 1). The correlation coefficient between the western Amundsen Sea SIE and SAT-PC1 (the latter is leading by approximately 4-month) is 0.61 at 99% confidence level (accounting for autocorrelations in both series, Figure 4a). All ice anomaly maxima correspond with the (four) maxima in SAT-PC1 representing cold (La Niña) central tropical Pacific anomalies. The ice responded well to the two warm events in the early 1980s and between 1992 and 1995, but failed to respond to the other two warm events (1983 and 1988). The regression line (Figure 4c) explains 37% of the total variance

between the two variables; the rms error is ~1˚ of latitude. Examination of the correlation between western Amundsen Sea SIE and SAT PC1 (Figure 4a) reveals that the largest contribution to the strong correlation between these two series occurs during extreme events. This suggests that extreme conditions in the tropics (especially cold conditions) likely trigger the large variations in the polar sea ice field. To test this, we repeat the correlation and regression analysis by admitting only data points that contribute more than 1% to the overall correlation. This "threshold regression" reduces the rms error to 0.8 degree of latitude (Figure 4d). The correlation restricted to these supercritical values reaches 0.93, indicating that the linear regression can explain 86% of the total variance when considering extreme events only. Therefore, we can hindcast extreme western Amundsen Sea ice conditions of the previous two decades quite well using temperature data four months in advance**.** In a similar manner, we can hindcast the ADP Index (defined by the difference between SIE anomalies in the two dipole centers; near 132°E and 24°E) using SAT-PC1 two months in advance. This linear regression explains 42% of the total variance. Again the hindcast is improved when we only consider the extreme cold and warm cases. This linear regression provides a prediction for ice conditions over a broader area than the previous one for the Western Amundsen Sea SIE.

Finally, we examine how the maximum SIE following ENSO events responds to the tropical forcing (Figure 5). The SIE in the dipole region responds to the tropical conditions much more regularly than the SIE in other regions. Also apparent is the fact that the SIE in the dipole regions responds more consistently to La Niña conditions than to El Niño conditions. The leading EOF mode of the SIE strikingly demonstrates the later phenomenon. This is consistent with previous studies showing that the atmospheric circulation in the South Pacific failed to respond to ENSO warm events consistently (Karoly, 1989; Houseago et al, 1998). The irregularity is likely caused by the varying evolution of El Niño events in the absence of a single canonical evolution (Harangozo, 2000). Our study shows that SIE anomalies more consistently respond to La Niña events than El Nino events. That makes the Antarctic Dipole most predictable during La Niña years. Currently, the tropical Pacific is in a normal condition with a weakly negative temperature

anomaly (after a La Niña event from 1999-2000). We expect that Antarctic sea ice will be slightly more than normal years in the Pacific basin and slight less than normal years in the Atlantic basin in the coming austral winter.

Discussions

We conclude that the ADP is the predominant interannually-varying signal within the Southern Ocean SIE and SAT fields. A weaker propagating component (less than one half of the ADP's magnitude) contributes to what appears to be the ACW. A simple linear regression allows good prediction of extreme sea ice conditions in the dipole region, especially during La Niña years.

Since the ACW and ADP have the same wavelength and similar period, they are likely related. Likely relationships include: (1) The ACW propagates through the area and excites the standing wave, and (2) the ADP is excited by extra-polar teleconnections and its anomaly is advected out of the dipole area by the Antarctic Circumpolar Current and/or air-sea-ice coupling processes. We favor the latter relationship for the following three reasons: (1) The eastern Pacific and Weddell Gyre regions are very sensitive to extra-polar climate (Yuan and Martinson, 2000), (2) the ADP in SIE can be predicted by extra-polar SAT reasonably well during extreme cold and warm years and (3) the magnitude of ADP variability is more than twice of the ACW.

Moreover, this study provides observational support to a modeling study (Rind et al, 2000) that presents a mechanism explaining the tropical-polar teleconnection. Specifically, Rind et al. (2000) show that ENSO-related anomalies in tropical SST invoke a meridional temperature gradient in the Pacific that alters the intensity of the Hadley Cell, manifested in a meridional shift of the subtropical jet (STJ). For warm events, the STJ moves equatorward, farther from the source of available potential energy in the frigid Antarctic. This leads to a reduction in cyclogenesis and polar storm intensity. Likewise, this same tropical Pacific perturbation introduces a zonal temperature gradient, perturbing the Walker Cell's Atlantic subsidence leading to an effective relaxation of the Atlantic Hadley Cell, poleward shift of the Atlantic STJ and increased cyclogenesis in the Weddell branch of the ADP. This intensifies the Weddell polar gyre, expanding the ice extent by increased equatorward divergence of the sea ice. The opposite happens with the spin down of the Amundsen

Sea circulation, thus explaining the presence of the ADP as a manifestation of hemispheric scale teleconnections between the tropics and polar regions. The results are also consistent with upper ocean Weddell gyre variability (Martinson and Iannuzzi, 2000). The leading modes of sea level pressure and temperature in our study clearly reveal the relatively weakened polar gyre in the Pacific, equatorward STJ associated with the warm events in the tropical Pacific and relatively stronger subpolar gyre in the Atlantic. The relationship between ENSO events and SIE anomaly in the dipole region is also consistent with the modeling results.

Acknowledgments: Support for this research was provided by a NASA grant NAGS-8725 and an environmental research grant by Ford Motor Company. The last part of the research was completed when Yuan was visiting the Chinese Academy of Meteorological Science. The sea ice concentration data were provided by NOAA's National Snow and Ice Data Center. Lamont contribution number xxxxx.

References

Carleton, A. M., Antarctic Sea-Ice Relationships with Indices of the Atmospheric Circulation of the Southern Hemisphere, *Climate Dynamics*, 3, 207-220, 1989.

Chiu, L. S., Antarctic Sea Ice Variations 1973-1980, In: Variations in the Global Water Budget, Street-Perrot et al., eds., Reidel Publ., Dordrecht, 301-311, 1983.

Harangozo, S.A.: A search for the ENSO teleconnections in the west Antarctic Peninsula climate in austral winter. *Int. J. Clim.*, 20, 663-679, 2000.

Horel, J. D., 1984: Complex principal component analysis: Theory and examples. *J. Climate and Applied Meteorology*, **23**, 1660-1673.

Houseago, R., G. McGregor, J.C. King and S.A. Harangozo: Climate Anomaly Wave-train Patterns Linking Southern Low and High Latitudes During South Pacific Warm and Cold Events. *Int. J. Climatol.* , **18**, 1181-1193.

Ledley, T. S. and Z. Huang, A Possible ENSO signal in the Ross Sea, Geophys., Res. Lett., 24, 3253-3256, 1997.

Kalnay E. et al. The NCEP/NCAR 40-year reanalysis project. *Bulletin of the American Meteorological Society*, 1996.

Martinson, D.G. and R.A. Iannuzzi, Spatial/Temporal Patterns in Weddell Gyre Characteristics and Their Relationship to Global Climate. *J. Geophys. Res.*, submitted (2000). [available at: http://rainbow.ldgo.columbia.edu/]

Rind., D., M. Chandler, J. Lerner, D. G. Martinson and X. Yuan, The Climate Response to Basin-Specific Changes in Latitudinal Temperature Gradients and The Implications for Sea Ice Variability, *J. Geophys. Res.*, in press [available at: http://rainbow.ldgo.columbia.edu/]

Simmonds, I. and T. H. Jacka, Relationships between the Interannual Variability of Antarctic Sea Ice and the Southern Oscillation, *J. Climate*, 8, 637-647, 1995.

Wallace, J. M. and R. E. Dickinson, 1972: Empirical Orthogonal Representation of time series in the frequency domain. Part I: Theoretical Considerations. *Journal of Applied Meteorology*, 11, 887-900.

White, B. W. and R. G. Peterson, 1996: An Antarctic circumpolar wave in surface pressure, wind, temperature and sea ice extent. *Nature*, **380**, 699-702.

Trenberth, K. and T.J. Hoar: The 190-1995 El Nino–Southern Oscillation. G. J. L., 23, 57-69, 1996.

Yuan, X. and D. G. Martinson, Antarctic Sea Ice Extent Variability and its Global Connectivity, *J. of Climate*, 3, 1697-1717, 2000.

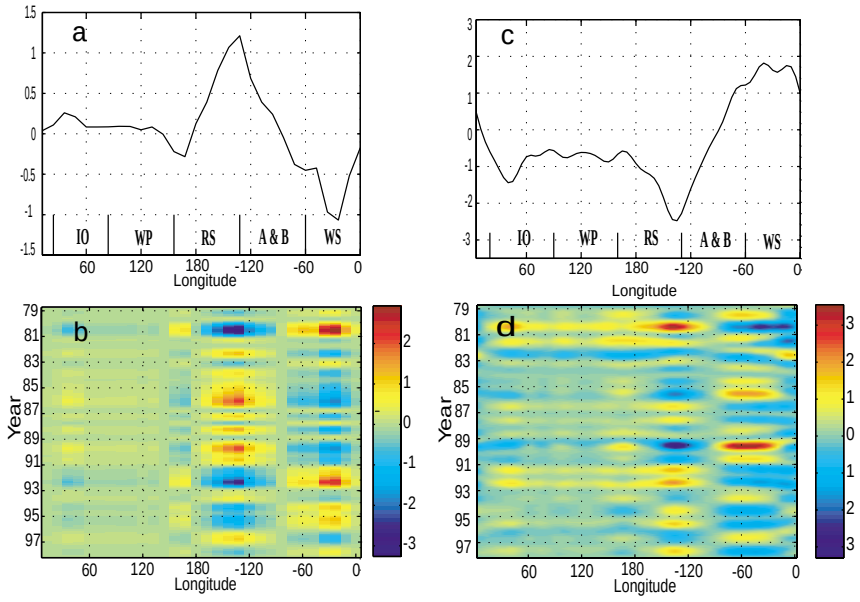

Figure 1. a: The eigenvector of the leading EOF mode of the SIE anomaly (from 10/78 to 3/98) around the Antarctic (37% of the total variance). b: The SIE anomaly containing only the first mode. c: Sum of eigenvectors from the first and second EOF modes of SAT anomaly along 65°S from 1975 to 1999 containing 53% of the total variance. d: The SAT anomaly along 65°S containing only first and second EOF modes.

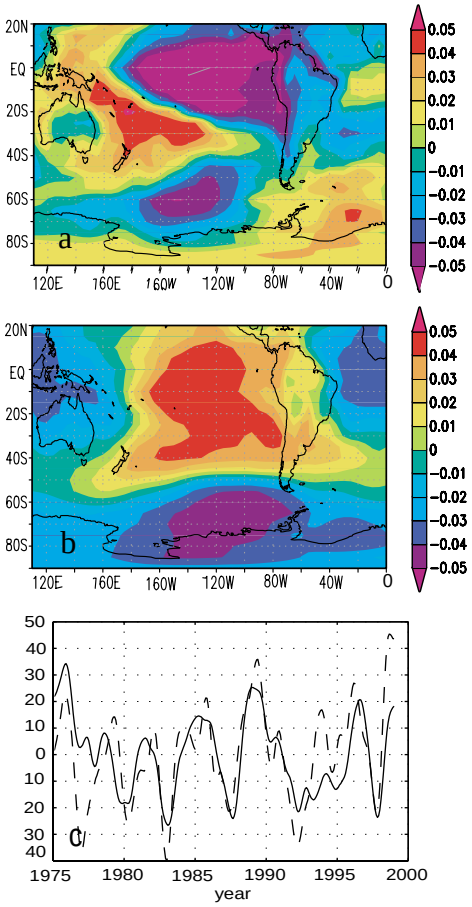

Figure 2. a: The leading EOF mode eigenvector of SAT anomaly from 1975 to 1999 containing 18% of the total variance. b: The leading EOF mode eigenvector of SLP containing 28% of the total variance in the same period as in figure 2a. c: The principle component of temperature and pressure (dashed line) leading modes.

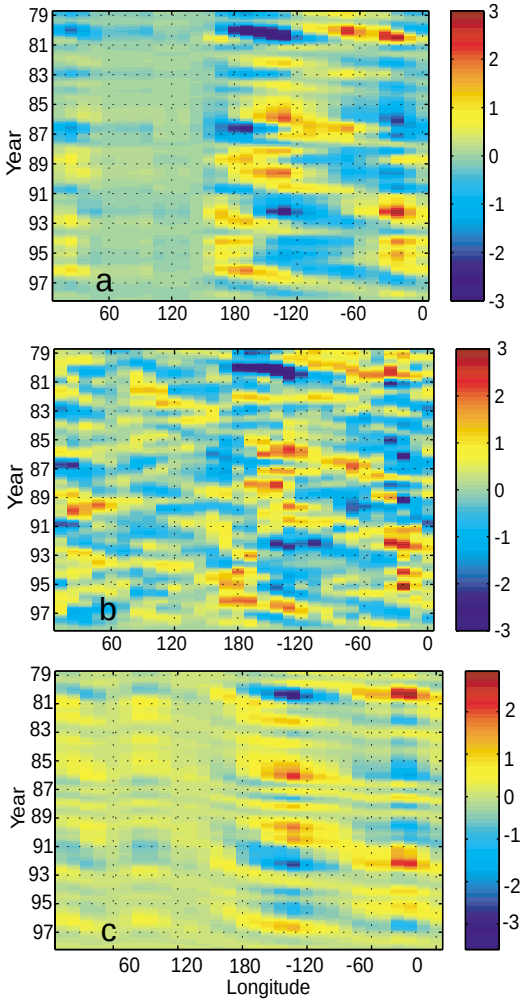

Figure 3. a: The SIE anomaly containing only first and second EOF modes (54% of total variance) as function of space and time. b: The SIE anomaly as function of space and time. c: The SIE anomaly containing only the first complex EOF mode (40% of the total variance).

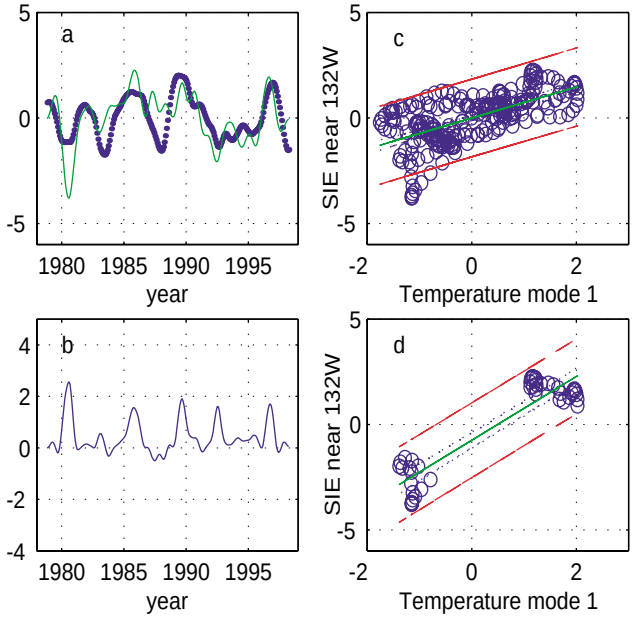

Figure 4. a: The SAT PC1 (dotted line) and the SIE anomaly near 132°W as function of time (SAT PC1 is shifted backward four months). b. Instantaneous correlation coefficients between the two curves in a measuring the contribution of the data at each time to the total correlation coefficient. c: A scatter plot of the SIE and SAT PC1 in a, and their linear regression. The 95% confidence levels for the points with for the regression line and for the individual point are marked. d: Same as c except for points with instantaneous correlation above 1%.

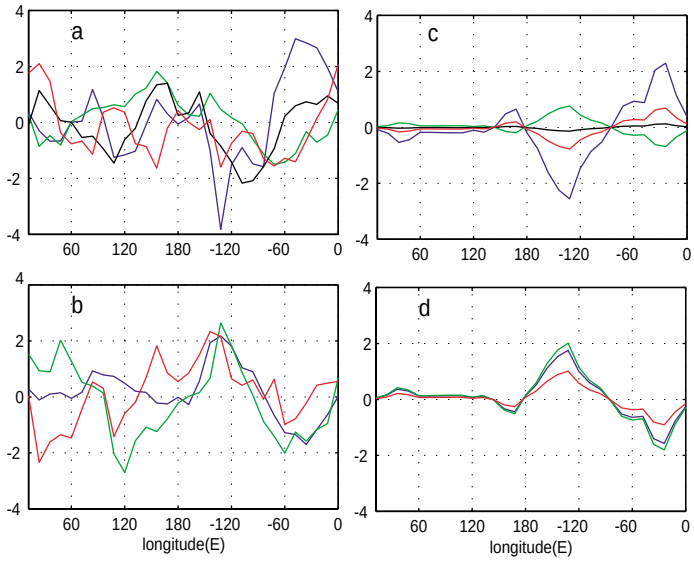

Figure 5. September (the maximum ice cover month in the Southern Hemisphere) SIE anomalies as function of longitude following four EL Nino events in 1980, 1983, 1988 and 1992 (a) and three La Nina events in 1985, 1989 and 1996 (b). In the same way, September SIE anomalies containing only the first EOF mode in the same El Nino years (c) and La Nina years (d).